 doi:10.20944/preprints201804.0235.v1

Peer-reviewed version available at *Processes* **2018**, *6*, 52; doi:10.3390/pr6050052

AN INTEGRATED APPROACH TO WATER-ENERGY NEXUS IN SHALE-GAS PRODUCTION

Fadhil Y. Al-Aboosi[a,b] and Mahmoud M. El-Halwagi[a,*]

[a]The Artie McFerrin Department of Chemical Engineering, Texas A&M University, College Station, Texas 77843-3122

[b]Department of Energy Engineering, Baghdad University, Baghdad, Iraq

ABSTRACT- Shale gas production is associated with significant usage of fresh water and discharge of wastewater. Consequently, there is a necessity to create the proper management strategies for water resources in shale gas production and to integrate conventional energy sources (e.g., shale gas) with renewables (e.g., solar energy). The objective of this study is to develop a design framework for integrating water and energy systems including multiple energy sources, cogeneration process, and desalination technologies in treating wastewater and providing fresh water for shale gas production. Solar energy is included to provide thermal power directly to a multi-effect distillation plant (MED) exclusively (to be more feasible economically) or indirect supply through a thermal energy storage system. Thus, MED is driven by direct or indirect solar energy, and excess or direct cogeneration process heat. The proposed thermal energy storage along with the fossil fuel boiler will allow for the dual-purpose system to operate at steady-state by managing the dynamic variability of solar energy. Additionally, electric production is considered to supply a reverse osmosis plant (RO) without connecting to the local electric grid. A multi-period mixed integer nonlinear program (MINLP) is developed and applied to discretize operation period to track the diurnal fluctuations of solar energy. The solution of the optimization program determines the optimal mix of solar energy, thermal storage, and fossil fuel to attain the maximum annual profit of the entire system. A case study is solved for water treatment and energy management for Eagle Ford Basin in Texas.

Keywords: Cogeneration, Process integration, Solar energy, Thermal storage, Desalination, Optimization

Peer-reviewed version available at Processes 2018, 6, 52; doi:10.3390/pr6050052

INTRODUCTION

Recently, major discoveries of shale gas reserves have led to substantial growth in production. For instance, the US production of shale gas has increased from 2 trillion ft^3 in 2007 to 17 trillion ft^3 in 2016 with estimated cumulative production of more than 400 trillion ft^3 over the next two decades [1]. Consequently, there are tremendous monetization opportunities to convert shale gas into value-added chemicals and fuels such as methanol, olefins, aromatics, and liquid transportation fuels [2-9]. A major challenge to a more sustainable growth of shale gas production is the need to address natural resource, environmental, and safety issues [10-11]. Specifically, the excessive usage of fresh water and discharge of wastewater constitute major problems. Hydraulic fracturing and horizontal drilling are the essential technologies to extract natural gas from shale rock. Water plays a significant role in shale gas production through mixing millions of gallons of water with sand, chemicals, corrosion inhibitors, surfactants, flow improvers, friction reducers, and other constituents to produce fracturing fluid. Under the high pressure, the fracturing fluid is injected into the wellbore to make cracks within the rock layers to increase the production [12-13]. Large quantities of water are used in the fracturing and related process [14]. The typical annual water consumption per well for hydraulic fracturing ranges between 1,000 and 30,000 m^3 leading to substantial amounts of water usage. For instance, the annual water usage in shale gas production is estimated to be about 120 MM m^3. In the Eagle Ford Shale Play, the annual water use is 18 MM m^3 for 1040 wells [15]. Wastewater associated with shale gas production is discharged in two forms: flowback water (which is released over several weeks following production) and produced water (which is the long-term wastewater) [14, 16]. Treatment of shale gas wastewater followed by recycle and reuse can provide major economic and environmental

Peer-reviewed version available at Processes 2018, 6, 52; doi:10.3390/pr6050052

benefits [12-17]. Regrettably, a small fraction of the shale-gas wastewater is recycled. A recent study [18] reported that in 2014, less than 10% of the roughly 80,000 wells in the US used recycled water after proper treatment. Lira-Barragán et al. [18] developed a mathematical programming model for the combination of water networks in the shale gas site by taking into consideration the requirement of water, the uncertainty of used and flowback water, and the optimal size of treatment units, storage systems, and disposals. Gao and You [12] addressed the shale-gas water problem as a mixed integer linear fractional programming (MILFP) problem to maximize the profit per unit of freshwater consumption. Yang et al. [14] developed a two-stage mixed integer linear programming (MINLP) model has been proposed for shale gas formations with the uncertainty of water availability. Several technologies may be used for treatment including thermal desalination and membrane separation [13–20]. These technologies require significant usage of thermal and/or electric energy. Some of the energy may be provided by shale gas, flared gases, or other on-site sources [21]. Additionally, renewable energy (such as solar) may be utilized to enhance the sustainability of the system. Therefore, it is important to consider the water management problem for shale gas production via a water-energy nexus framework.

This work is aimed at developing a new systematic approach to design, operation, integration, and optimization of a dual-purpose system which integrates solar energy and fossil fuels for producing electricity and desalinated water while treating shale-gas wastewater. In addition to fossil fuels, a concentrated solar power field, a thermal storage system, conventional steam generators, and cogeneration process are coupled with two water treatment plants: reverse osmosis (RO) and multiple-effect distillation (MED). A multi-period mixed integer nonlinear program (MINLP) formulation is developed to account for the diurnal fluctuations of solar energy.

Peer-reviewed version available at *Processes* **2018**, *6*, 52; doi:10.3390/pr6050052

The solution of the mixed integer nonlinear program (MINLP) determines the optimal mix of solar energy, thermal storage, and fossil fuel and the details of wastewater treatment and water recycle.

PROBLEM STATEMENT

Consider a shale-gas production site with the following known information:

- Flowrate and characteristics of produced and flared shale gas.
- Demand for fresh water (flowrate and quality).
- Flowrate and characteristics of flowback and produced wastewater.

The site is not connected to an external power grid.

It is desired to systematically design an integrated system which:

- Treats the wastewater for on-site recycle/reuse.
- Uses solar energy and fossil fuels to provide the needed electric and thermal power needs.
- Satisfies technical, economic, and environmental requirements.

Given are:

- Flowrate and composition of shale gas (sold and flared).
- Flowrate and purity needs for fresh water.
- Total volumetric flow of wastewater (flow-back and produced water) of shale gas play.
- Flowrate of flared gases that may be used in the cogeneration process.
- Electric energy requirement for RO and MED, (kWh_e/m^3).
- Thermal energy requirement for MED, (kWh_t/m^3).

To solve the problem, the following questions should be addressed:

Peer-reviewed version available at Processes 2018, 6, 52; doi:10.3390/pr6050052

- What the maximum annual profit of the whole system for producing desalinated water, electricity for the various percentage contribution of RO and MED in the total desalinated water production?
- What the minimum total annual cost of the entire system?
- What is the economic feasibility of the system?
- What is the optimal mix of solar energy, thermal storage, and fossil fuel for MED plant and the entire system?
- What is the optimal design and integration of the system?
- What are the optimal values of the design and operating variables of the system (e.g., minimum area of a solar collector, maximum capacity of a thermal storage system, etc.)?
- What is the feasible range of the percentage contribution of RO and MED in the total desalinated water production?

The Superstructure integrates primary components of solar energy and fossil fuels for producing electricity and desalinated water, as shown in Figure 1:

- To achieve a steady supply of thermal power to the whole system, solar energy (as direct solar thermal power), fossil fuel (shale gas, flared gas), and a thermal energy storage (as indirect solar thermal power) are used.
- Solar energy is used as a source of heat to provide thermal power directly to MED plant exclusively (to be more economically feasible), while the surplus thermal power is stored.
- A two-stage turbine is used to enhance the cogeneration process efficiency.

Preprints (www.preprints.org) | NOT PEER-REVIEWED | Posted: 18 April 2018 doi:10.20944/preprints201804.0235.v1

Peer-reviewed version available at Processes 2018, 6, 52; doi:10.3390/pr6050052

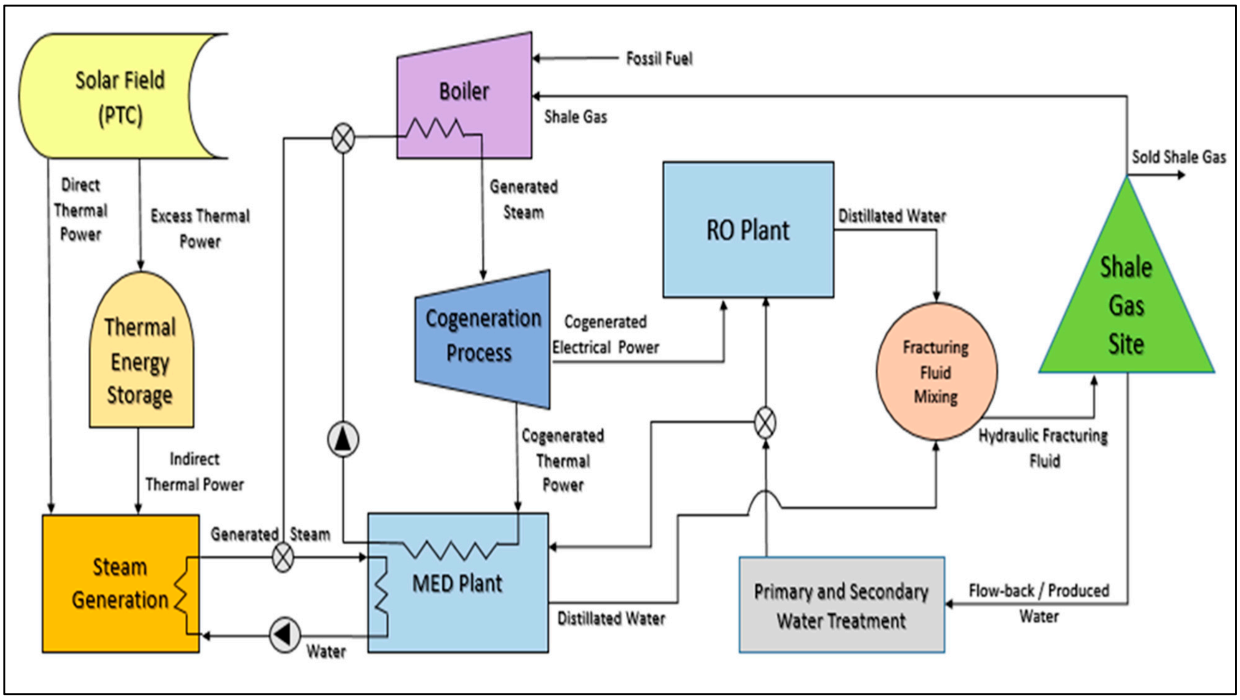

Figure 1: Proposed Superstructure Representation

APPROACH

A hierarchical design is proposed to efficiently address the water-energy nexus problem. Figure 2 demonstrates the main steps of the approach. The first step is to gather the required data for the system then to select and formulate the appropriate models that describe the major system components. Once the preceding steps are achieved, the computational optimization is applied to the integrated system to maximize annual profit of the system that produces a specific level of desalinated water and electricity. To decompose the optimization problem, the percentage contribution of RO and MED to treating wastewater is iteratively discretized. For each discretization, the thermal and electric loads are calculated, and the energy systems are optimized and designed. The total annualized cost for each discretized iteration is calculated and finally the minimum-cost solution is selected.

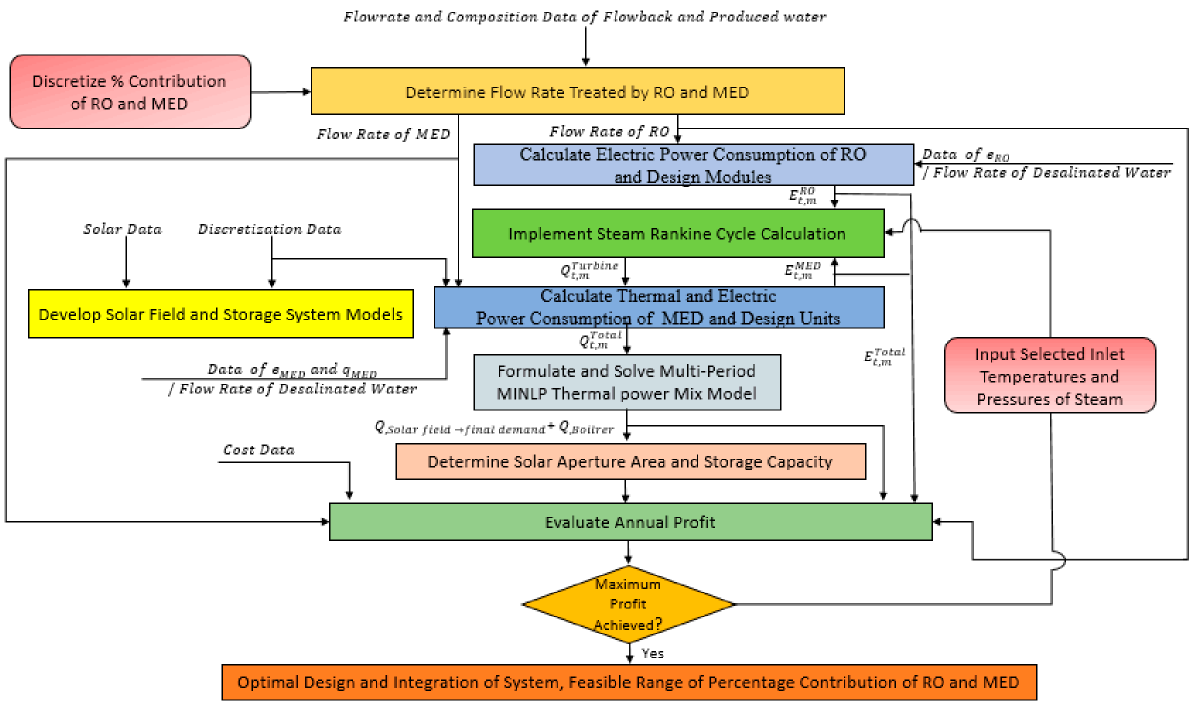

Figure 2: Proposed approach

Modeling the Building Blocks

The performance models for MED and RO have been taken from literature [22-26]. For the solar system, a parabolic trough collector was selected. The modeling of the solar system was based on literature models and data [27-30] as described in this section. The solar thermal power (per unit length of a collector) that produced by the solar field when the direct normal irradiance (DNI) strikes collector aperture plane is given by the following expression:

$$Q_{sun \to collector}(W/m) = DNI.\cos\Theta.W_c \tag{1}$$

where DNI (W/m^2) is the direct normal irradiance, Θ is the solar incidence angle, W_c (m) is the width of the collector aperture.

Preprints (www.preprints.org) | NOT PEER-REVIEWED | Posted: 18 April 2018 doi:10.20944/preprints201804.0235.v1

Peer-reviewed version available at *Processes* **2018**, *6*, 52; doi:10.3390/pr6050052

For North-South orientation, the incidence angle is calculated as follows:

$$\cos \Theta = \sqrt{cos^2 \Theta_z + cos^2 \delta . sin^2 \omega} \quad (2)$$

where Θ_z is the solar zenith angle, δ is the declination, ω is the hour angle.

To calculate the thermal power (per unit length of a collector) that absorbed by the receiver tube of a collector loop, the influences of the optical losses can be taken into consideration by inserting four parameters to Eq. is given by the following expression:

$$Q_{collector \rightarrow reciever}(W/m) = DNI. \cos \Theta . W_c . \eta_{opt} . K(\Theta). F_f . R_{SL} . O_{EL} \quad (3)$$

Where η_{opt} is the peak optical efficiency of a collector, $K(\Theta)$ is the incidence angle modifier, F_f is the soiling factor (mirror cleanliness), R_{SL} is the row shadow loss, O_{EL} is the optical end loss.

The peak optical efficiency of a collector when the incidence angle on the aperture plane is 0° is:

$$\eta_{opt} = \rho . \gamma . \tau . \alpha \big|_{\Theta = 0^o} \quad (4)$$

where ρ is the reflectivity, γ is the intercept factor, τ is the glass transmissivity, α is the absorptivity of the receiver pipe.

The incidence angle modifier for an LS-3 collector is given by:

$$\begin{aligned} K(\Theta) &= 1 - 2.23073 \times 10^{-4} . \Theta - 1.1 \times 10^{-4} . \Theta^2 + 3.18596 \times 10^{-6} . \Theta^3 \\ &\quad -4.85509 \times 10^{-8} . \Theta^4 \qquad 0^0 \le \Theta \le 80^0 \\ K(\Theta) &= 0 \qquad \Theta > 80^o \end{aligned} \quad (5)$$

Peer-reviewed version available at Processes 2018, 6, 52; doi:10.3390/pr6050052

The row shadow factor is:

$$R_{SL} = min\left[\max\left(0.0, \frac{L_{spacing}}{W_c} \cdot \frac{\cos\Theta_z}{\cos\Theta}\right); 1.0\right] \quad (6)$$

where $L_{spacing}(m)$ is length of spacing between troughs.

The optical end loss is:

$$O_{EL} = 1 - \frac{f.\tan\Theta}{L_{SCA}} \quad (7)$$

where f is focal length of the collectors (m), L_{SCA} is length of a single collector assembly (m).

The total thermal power (per unit length of a collector) that loss from a collector represents the combination of the radiative heat loss from the receiver pipe to ambient ($Q_{reciever \to ambient}$) and convective and conductive heat losses from the receiver pipe to its outer glass pipe ($Q_{receiver \to glass}$), *and* is calculated by the following expression:

$$Q_{collector \to ambient}\,(W/m) = U_{rec}\,.\,\pi\,.\,d_o\,.\,(T_{rec} - T_{amb}) \quad (8)$$

where U_{rec} $(W/m^2_{rec}\,.\,K)$ is the overall heat transfer coefficient of a receiver pipe, d_0 (m) is the outer diameter of a receiver pipe, T_{rec} (K) is the mean receiver pipe temperature, $T_{amb}(K)$ is the ambient air temperature.

The overall heat transfer coefficient of a collector is found experimentally depending on a receiver pipe temperature, and it can be given in the second-order polynomial equation:

$$U_{rec} = a + b\,(T_{rec} - T_{amb}) + c\,(T_{rec} - T_{amb})^2 \quad (9)$$

where a, b, and c coefficients have been calculated experimentally for the LS-3 collector have been reported in literature [27].

Preprints (www.preprints.org) | NOT PEER-REVIEWED | Posted: 18 April 2018 doi:10.20944/preprints201804.0235.v1

Peer-reviewed version available at *Processes* **2018**, *6*, 52; doi:10.3390/pr6050052

The thermal power (per unit length of a collector) that transferred from a collector to a fluid is given in the following expression [31]:

$$Q_{collector\rightarrow fluid}(W/m) = Q_{collector\rightarrow receiver} - Q_{collector\rightarrow ambient} \quad (10)$$

The thermal power (per unit length of a collector) that loss from the headers (pipes) is given in the following expression [32]:

$$Q_{LFP}(W/m) = 0.0583 \,.\, W_c.\,(T_{rec} - T_{amb}) \quad (11)$$

The thermal power (per unit length of a collector) that loss from the expansion tank (vessel) is given in the following expression [32]:

$$Q_{,LFV}(W/m) = 0.0497 \,.\, W_c.\,(T_{rec} - T_{amb}) \quad (12)$$

The useful thermal power (per unit length of a collector) that produced by the solar field is given by the following expression, which represents the sum of Equations 10-12:

$$Q_{solar\ field\rightarrow final\ demand}(W/m) = Q_{collector\rightarrow receiver} - Q_{collector\rightarrow ambient} - Q_{LFP} - Q_{LFV} \quad (13)$$

The inlet thermal power of the thermal storage is given in the following expression:

$$Q_{in} = m_{ms} \,.\, C_{P,ms} \,.\, (T_{HT} - T_{CT}) = \eta_{EX} \,.\, m_{oil} \,.\, C_{P,oil} \,.\, (\Delta T) \quad (14)$$

And the expression of the discharge process (outlet thermal power) is given by:

$$Q_{out} = m_{oil} \,.\, C_{P,oil} \,.\, (\Delta T) = \eta_{EX} \,.\, m_{ms} \,.\, C_{P,ms} \,.\, (T_{HT} - T_{CT}) \quad (15)$$

where m_{ms} is the molten salt flow rate (kg/s), ($C_{P,ms}$ = $1443 + 0.172\ T_{ms}$) is the specific heat of the molten salt $(J/kg.^{\circ}C)$, T_{ms} is the temperature $(^{\circ}C)$ of the molten salt, T_{HT} is the hot tank

Peer-reviewed version available at *Processes* **2018**, *6*, 52; doi:10.3390/pr6050052

temperature ($^{\circ}C$), T_{CT} is the cold tank temperature ($^{\circ}C$), η_{EX} is the efficiency of the heat exchanger, m_{oil} is the oil mass flowrate (Kg/s), ΔT is the difference between inlet and outlet of the oil.

The net thermal power inside the tank (W) can be calculated by the following expression:

$$Q_{TES} = Q_{acc} + Q_{in} - Q_{out} - Q_{loss} \tag{16}$$

where Q_{acc} is the accumulated thermal power in the tank from preceding iterations, Q_{loss} is the thermal power loss (kW/m^2) of the cold and heat tanks and it is given in the following empirical equation [33]:

$$Q_{loss} = 0.00017.T_{ms} + 0.012 \tag{17}$$

where T_{ms} is the temperature ($^{\circ}C$) of the molten salt in the hot and in the cold tanks.

The optimal values of the Rankine cycle parameters of cogeneration process can be satisfied by formulated the entire cycle as an optimization problem. Thus, there is a necessity to obtain suitable correlations of thermodynamic properties that can be used in optimization formulations. In thermodynamic calculations of the Rankine cycle, mathematical equations are used to replace the steam tables because they could incorporate easily into optimization formulations. However, available correlations for steam tables are complicated (e.g., nonlinear, nonconvex function), and it is hard to insert them in optimization task. Consequently, a new set of thermodynamic correlations have been developed in literature [34] to estimate properties of steam and they can be incorporated easily into optimization formulation and cogeneration design. The isentropic efficiency of the steam turbine can be obtained from the turbine hardware model, which developed by Mavromatis and Kokossis [35], to show the efficiency variation with the load, the turbine size, and operating conditions, as in the following correlation:

Preprints (www.preprints.org) | NOT PEER-REVIEWED | Posted: 18 April 2018 doi:10.20944/preprints201804.0235.v1

Peer-reviewed version available at *Processes* **2018**, *6*, 52; doi:10.3390/pr6050052

$$\eta_{is} = \frac{6}{5\,.\,B}\left(1 - \frac{3.41443\,.\,10^{6}\,.\,A}{\Delta h_{is}\,.\,m^{max}}\right)\left(1 - \frac{m^{max}}{6\,.\,\dot{m}}\right) \tag{18}$$

where $\dot{m}$ is the inlet turbine steam flowrate (Ib/hr), and m^{max} is the maximum mass flowrate of a turbine(Ib/hr) , A and B are parameters that depend on the inlet saturation temperature $(°F)$ and the type of turbine as in the following correlations:

$$A = a_o + a_1\,.\,T_{sat} \tag{19}$$

$$B = a_2 + a_3\,.\,T_{sat} \tag{20}$$

where a_o, a_1, a_2, a_3 the correlation constants and can be found in literature [36].

OPTIMIZATION FORMULATION

Because of the diurnal nature of solar energy, a multi-period approach is adopted. The annual operation is discretized in a number of operational periods (e.g., monthly). The index m refers to the operational period. For each operational period, an average meteorological day is used to represent the solar intensity data. In turn, the meteorological day is discretized into a number of sub-periods (e.g., 24 hours) where the index t is used to designate a sub-period. Two water-treatment technologies are used: multi-effect distillation (MED) and reverse osmosis (RO). MED consumes mostly thermal energy and some electric energy which are respectively given by the specific requirements: q_{MED} (kWh_t/m^3) and e_{MED} (kWh_e/m^3). RO requires electric energy which is represented by the following specific energy consumption term: e_{RO} (kWh_e/m^3).

For each sub-period t, the thermal power needs for water treatment is obtained directly from the combustion of fossil fuels ($Q_{t,m}^{Fossil}$), directly from a solar thermal collector ($Q_{t,m}^{Direct,SC}$),

Peer-reviewed version available at Processes 2018, 6, 52; doi:10.3390/pr6050052

indirectly from solar energy through thermal storage ($Q_{t,m}^{Out\_Stored\_SC}$), and from steam leaving the cogeneration turbine ($Q_{t,m}^{Turbine}$). Hence,

$$Q_{t,m}^{Total} = Q_{t,m}^{Fossil} + Q_{t,m}^{Direct,SC} + Q_{t,m}^{Out\_Stored\_SC} + Q_{t,m}^{Turbine} \qquad \forall t, \forall m \qquad (21)$$

where

$$Q_{t,m}^{Total} = F_{t,m}^{MED} q_{MED} \qquad \forall t, \forall m \qquad (22)$$

The electric power provided by the cogeneration turbine is given by:

$$E_{t,m}^{Total} = F_{t,m}^{RO} e_{RO} + F_{t,m}^{MED} e_{MED} \qquad \forall t, \forall m \qquad (23)$$

The thermal power captured by the solar collector ($Q_{t,m}^{SC}$) is directly used ($Q_{t,m}^{Direct,SC}$) or is stored ($Q_{t,m}^{In\_Stored-SC}$) for subsequent usage, i.e.

$$Q_{t,m}^{SC} = Q_{t,m}^{Direct,SC} + Q_{t,m}^{In\_Stored-SC} \qquad \forall t, \forall m \qquad (24)$$

Over a sub-period, *t,* the thermal power balance for the thermal storage unit is given by:

$$Q_{t,m}^{Stored-SC} = Q_{t-1,m}^{Stored-SC} + Q_{t,m}^{In\_Stored-SC} - Q_{t,m}^{Out\_Stored-SC} - Q_{t,m}^{Stored-Loss} \qquad \forall t, \forall m \qquad (25)$$

Such collected energy is a function of the solar-radiation intensity ($Solar\_Radiation_{t,m}$) and the effective surface area of the solar collector (A^{SC}).

Although each period requires a certain area of the solar collector, the design value (which is also used for capital cost estimation) is the largest of all needed areas, i.e.:

$$A_{t,m}^{SC} \leq A_{Design}^{SC} \qquad \forall t, \forall m \qquad (26)$$

Preprints (www.preprints.org) | NOT PEER-REVIEWED | Posted: 18 April 2018 doi:10.20944/preprints201804.0235.v1

Peer-reviewed version available at Processes 2018, 6, 52; doi:10.3390/pr6050052

The cogeneration turbine is modelled through a performance function (e.g., isentropic expansion with an efficiency) that combines inlet and outlet steam conditions and relates the produced power to heat.

$$\Omega_{t,m}^{Turbine}\left(D_{t,m}^{Tutbine}, O_{t,m}^{Turbine}, Steam_{t,m}^{In}, Steam_{t,m}^{Out}, Power_{t,m}^{Out}\right) = 0 \quad \forall t, \forall m \tag{27}$$

The objective function seeks to maximize the profit for the water-energy nexus system:

Maximize Annual Profit = Annual value of treated water + Annual value of avoided cost of discharging wastewater – Cost of fossil fuels - Total annualized cost of solar collection system – Total annualized cost of solar storage system – Total annualized cost of cogeneration system - Total annualized cost of MED system – Total annualized cost of RO system

Maximum Annual profit =

$$\begin{aligned}\sum_m \sum_t \left(v_{t,m}^{RO} F_{t,m}^{RO} + v_{t,m}^{MED} F_{t,m}^{MED}\right) + c^{Waste} W_w - \sum_m \sum_t \left(c_{t,m}^{Fossil} F_{t,m}^{Fossil}\right) - AFC^{SC} \\ - \sum_m \sum_t OPEX_{t,m}^{SC} - AFC^{SC\_Storage} - \sum_m \sum_t OPEX_{t,m}^{SC\_Storage} - AFC^{Cogen} \\ - \sum_m \sum_t OPEX_{t,m}^{Cogen} - AFC^{MED} - \sum_m \sum_t OPEX_{t,m}^{MED} - AFC^{RO} - \sum_m \sum_t OPEX_{t,m}^{RO}\end{aligned} \tag{28}$$

CASE STUDY

To demonstrate the viability of the proposed approach for solution strategies, a case study will be solved that based on the Eagle Ford shale play, which is located south Texas. A dual-purpose system which integrates solar energy and fossil fuels for producing electricity and fresh water has been considered. The optimal design, operation, and integration of the system will be found through this case study that requires particular input data for each unit of the entire system. As mentioned earlier, this system includes concentrated solar power field, a thermal storage

Preprints (www.preprints.org) | NOT PEER-REVIEWED | Posted: 18 April 2018 doi:10.20944/preprints201804.0235.v1

Peer-reviewed version available at Processes 2018, 6, 52; doi:10.3390/pr6050052

system, conventional steam generators, and a cogeneration process into two water treatment plants, a reverse osmosis plant (RO) and a multiple-effect distillation plant (MED).

Flowback/Produced Water of Shale Gas Play

In order to supply a specific amount of flow-back and produced water (FPW) from a shale play to a desalination plant, the calculation of an FPW flow average for many years is an appropriate option to avoid the uncertainty in the amount of FPW. Specifically, if we know that wastewater of shale play is typically subjected to heavily regulated and should store in containers so that these containers can be utilized to get a constant flow approximately. Additionally, a large number of wells in a shale play can contribute to making the flow rate of FPW approximately constant because when the FPW production of one well starts declining, another well will start its production and compensate a drop of production in other wells.

Table 1 shows the estimated value of flowback and produced water that returned from shale gas formations to the surface in the Eagle Ford basin. This estimated value is based on the study [37] for 10 plays since the early 2000s until 2015.

Table I: Estimated numbers of shale gas wells in Eagle Ford Basin [37]

Shale gas formations	Number of wells	Total water use $10^6 m^3$	Total gas production $(10^{12} ft^3)$	Total oil production $(10^6 bbl)$	Total FPW $10^6 m^3$
Eagle ford	5846	80.08	8.01	723.52	151.22

Preprints (www.preprints.org) | NOT PEER-REVIEWED | Posted: 18 April 2018 doi:10.20944/preprints201804.0235.v1

Peer-reviewed version available at Processes 2018, 6, 52; doi:10.3390/pr6050052

The techno-economic data for RO and MED are reported in Table 2.

Table 2. Techno-Economic Data for RO and MED [22, 38]

Technology	Thermal energy consumption ($kWht/m^3$ Desalinated water)	Electric energy consumption ($kWhe/m^3$ Desalinated water)	Annualized fixed cost (AFC) ($\$/year$)	Operating cost ($\$/m^3$ $seawater$)	Water recovery (m^3 desalinated water/m^3 feed seawater)	Value of desalinated water ($\$/m^3$ desalinated water)	Outlet Salt Content (ppm)
RO	-	4	$2.0 \,.\, 10^6 + 1{,}166 \,.\, (flowrate\ of\ seawater, m^3/day)^{0.8}$	0.18	0.55	0.88	200
MED	65	2	$13.0 \,.\, 10^6 + 2{,}227 \,.\, (flowrate\ of\ seawater, m^3/day)^{0.7}$	0.24	0.65	0.82	80

Solar Energy

The solar data are summarized in Appendix I. Table 3 summarizes the main cost data for the solar collectors.

Table 3: The direct capital cost of parabolic trough collector items [39, 40]

Item	Receivers	mirrors	Concentrator Structure	Concentrator Erection	Drive	Piping
Cost $\$/m^2$	43	40	47	14	13	10
Item	Electronic &control	Header piping	Civil works	Spares, HTF, Freight	Contingency	Structures &Improvement
Cost $\$/m^2$	14	7	18	17	11	7

Preprints (www.preprints.org) | NOT PEER-REVIEWED | Posted: 18 April 2018 doi:10.20944/preprints201804.0235.v1

Peer-reviewed version available at Processes 2018, 6, 52; doi:10.3390/pr6050052

The total fixed capital cost of the solar field ($) is the sum of heat collection element (HCE), mirror, support structure, drive, piping, civil work, structures, and improvements, as follows:

$$FCI_{SF} = C_{SF} \,.\, A_{SF} \tag{29}$$

where C_{SF} is the solar field cost per area unit ($\$\, 241/m^2$), A_{SF} is the solar field aperture area (m^2).

The thermal storage system is assumed an indirect two-tank type which is used the binary solar salt (sodium and potassium nitrate) as a storage material with the following fixed capital cost estimation ($):

$$FCI_{TES} = C_{TES} \,.\, SC \,.\, Q_{solar\ field \rightarrow final\ demand} \tag{30}$$

where C_{TES} is the thermal storage system cost per thermal energy unit ($\$27.18/kWh$), SC is the number of storage capacity hours (hr), $Q_{solar\ field \rightarrow final\ demand}$ is the useful thermal power that produced by solar field (kW).

The fixed capital cost estimation of a steam generator system ($) is calculated as:

$$FCI_{SG} = C_{SG} \,.\, Q_{solar\ field \rightarrow final\ demand} \tag{31}$$

where C_{SG} is the steam generator system cost per thermal power unit ($\$/kW_t$).

The fixed capital cost of a boiler ($), which is assumed a water-tube boiler fueled with gas or oil, is estimated as follows [34]:

$$FCI_B = 3 \,.\, N_p \,.\, N_T \,.\, Q_{Boiler}^{0.77} \tag{32}$$

where Q_{Boiler} is the amount of thermal power (BTU/hr) transferred to the steam and equal to (Q_{Boiler}/η_{boiler}), η_{boiler} is the efficiency of a boiler, N_P is a factor to account for the operation

Peer-reviewed version available at Processes 2018, 6, 52; doi:10.3390/pr6050052

pressure and it is given by: $N_P = 7\,.\,10^{-4}.\,P_g + 0.6$; P_g is the gauge pressure (pisg) of a boiler, N_T is a factor accounting for the superheat temperature and is given by:

$N_T = 1.5\,.\,10^{-6}\,.\,T_{SH}^2 + 1.13\,.\,10^{-3}\,.\,T_{SH} + 1$; T_{SH} is the superheat temperature (°F), $T_{SH} = T^{in} - T_{sat}^{in}$; T^{in} is the temperature at the inlet of a turbine, T_{sat}^{in} is the saturation temperature at the inlet of a turbine.

The fixed capital cost of a turbine ($), which is assumed a non-condensing turbine, is estimated as follows [34]:

$$FCI_T = 475\,.\,E_T \tag{33}$$

where $E_{,T}$ is the turbine shaft power output (BTU/hr); $E_{,T} = m\,.\,(h^{in} - h_{act}^{out})$.

Flared Gas

The shale gas production from Eagle Ford wells can be used as a fuel for cogeneration process. Furthermore, the flared gas can be used also as a fuel source for cogeneration process that it will contribute to saving a considerable amount of shale gas along with diminishing CO_2 emissions accompanying to the flared gas. In Eagle Ford fields, 4.4 billion cubic feet of gas was flared in 2013 that represented around 13% of the gas in the formation [41].

Total Cost

The annual fixed cost (AFC) ($\$/year$) of the system is determined as follows:

$$\text{AFC} = [(FCI_{SF} + FCI_{TES} + FCI_{SG} + FCI_B + FCI_T + FCI_{PST})/N] + AFC_{RO} + AFC_{MED} \tag{34}$$

Peer-reviewed version available at Processes 2018, 6, 52; doi:10.3390/pr6050052

The operation and maintenance cost ($\$/hr$) of solar field, cogeneration process, thermal storage system, administration, and operations is estimated as follows, based on data are given by [39, 40]:

$$OC_{OM} = C_{OM} \cdot \left(Q_{solar\ field \to final\ demand} + Q_{Boiler}\right) \tag{35}$$

where C_{OM} is the operation and maintenance cost per thermal power unit ($\$0.0203/kWh$).

The type and amount of the selected fuel are necessary to estimate the cost of fuel ($\$/hr$) and it is formulated as follows:

$$OC_F = C_F \,.\, Q_B \,.\, 3413 \,.\, 10^{-6} \tag{36}$$

where C_F is the fuel cost ($\$/MMBTU$), Q_B is the amount of thermal power (BTU/hr) that equals to (Q_{Boiler}/η_{boiler}), η_{boiler} is the efficiency of a boiler.

The annual operating cost (AOC) ($\$/year$) is determined as follows:

$$AOC = a_Y \,.\, (OC_{OM} + OC_F) \tag{37}$$

where a_Y is the annual operation time ($hr/year$).

The annual income ($\$/year$) is the sum of the total desalinated water production value and the saving value of a reduction in the cost of transportation, fresh water acquisition, and disposal:

$$Annual\ income = a_Y \,.\{(0.88 \,.\, flowrate\ of\ desalinted\ water\ from\ RO, m^3/hr + 0.82 \,.\, flowrate\ of\ desalinted\ water\ from\ MED, m^3/hr) + [(C_{FW} + C_{DS} + C_{TR}) \,.\, total\ flowrate\ of\ disalinated\ water\ from\ (RO, MED)]/0.11924\} \tag{38}$$

Peer-reviewed version available at Processes 2018, 6, 52; doi:10.3390/pr6050052

where C_{FW} is the fresh water cost per volume unit($0.24\$/bbl$), C_{DS} is the disposal cost per volume unit($0.05\$/bbl$), C_{TR} is the transportation cost per volume unit($0.89\$/bbl$).

The net profit represents the sum of the total desalinated water production value and the saving value of a reduction in the cost of transportation, fresh water acquisition, and disposal. The treatment process of flowback and produced water in a shale gas site that can be contributed effectively to save a money for each barrel of flowback and produced water which should be trucked and disposed. Table 4 shows the cost of transportation, fresh water acquisition, primary /secondary treatment, and disposal depending on the characteristics of a water treatment plant with capacity a 2,380 $barrel/day$ in Eagle Ford basin [42].

Table 4: Cost of transportation, fresh water, treatment, and disposal of FPW

Fresh water ($\$/barrel$)	0.24
Disposal (Deep well + Landfill) ($\$/barrel$)	0.05
Primary & secondary treatment ($\$/barrel$)	0.34
Transportation ($\$/barrel$)	0.89

RESULTS & DISCUSSION

A detailed performance model of the parabolic trough was applied to the case study to determine the useful thermal power (per unit length of a collector) that produced by the solar field. The calculations of the solar field have been carried out depending on the monthly average of hourly direct solar irradiance, hourly ambient temperature, and hourly incidence angle. Moreover, the characteristics of the LS-3 collector were adopted and all types of thermal losses (convection, conduction, radiation) are considered for the entire the solar field. The hourly variations in the useful thermal power for 12 months were obtained, as shown in Figure 3.

Peer-reviewed version available at *Processes* **2018**, *6*, 52; doi:10.3390/pr6050052

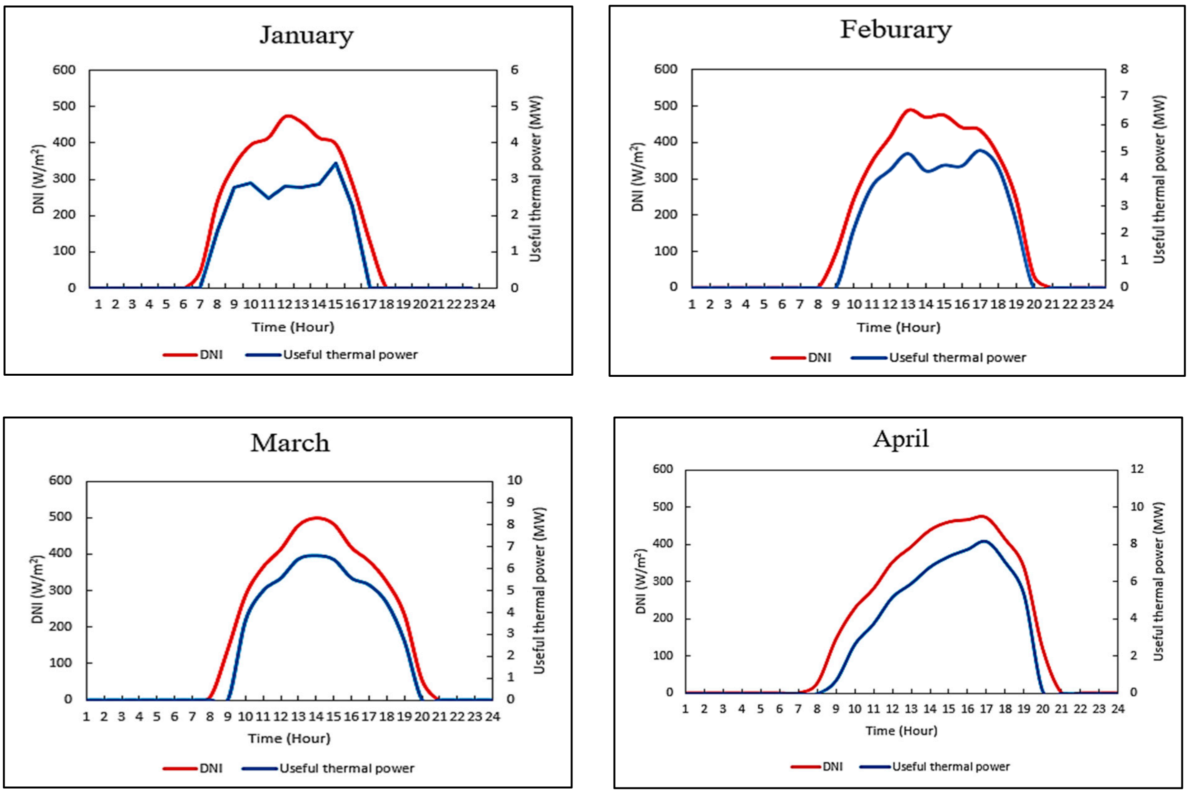

doi:10.20944/preprints201804.0235.v1

Peer-reviewed version available at Processes 2018, 6, 52; doi:10.3390/pr6050052

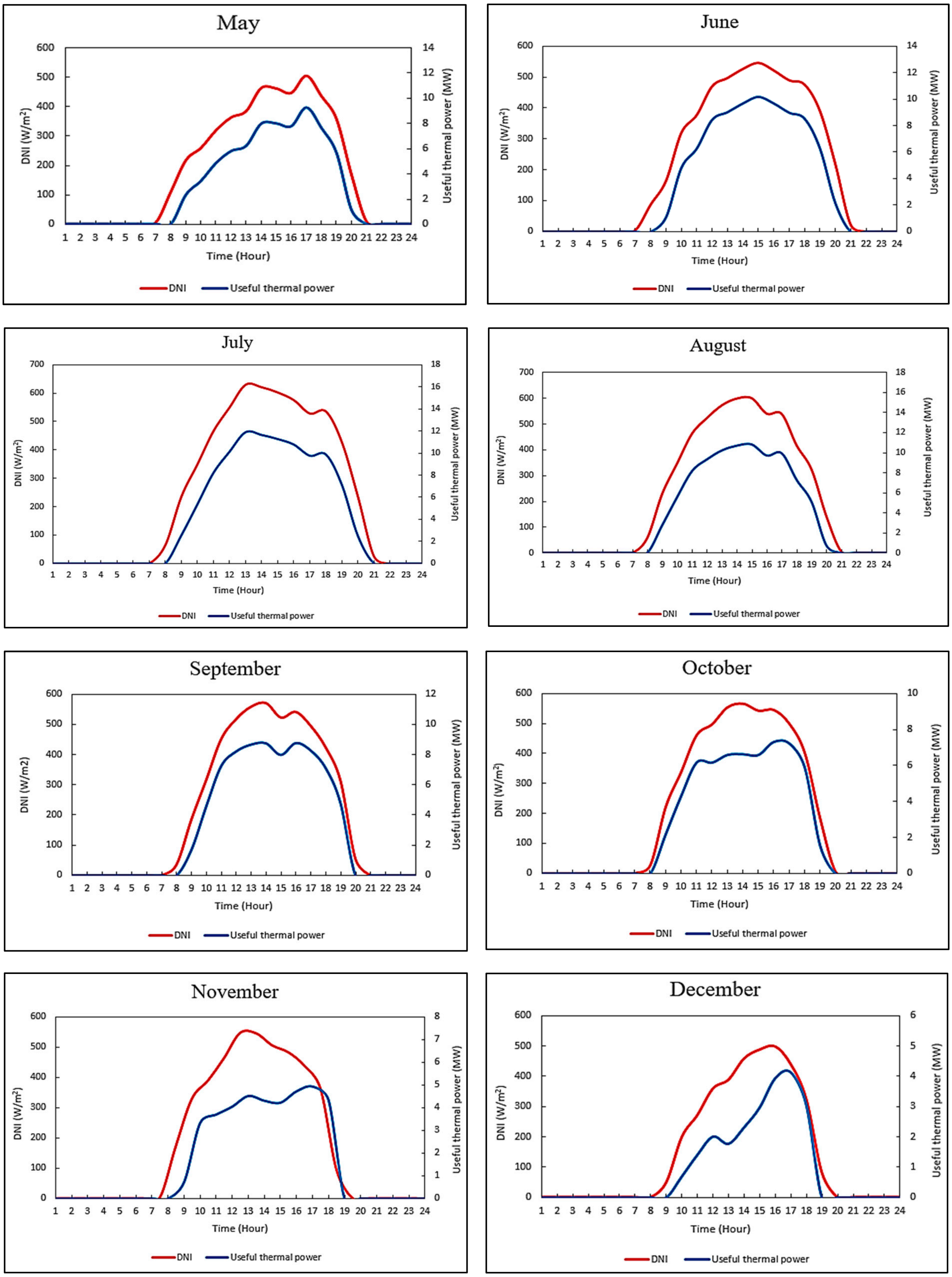

Figure 3: Monthly average of hourly DNI and useful thermal power

Preprints (www.preprints.org) | NOT PEER-REVIEWED | Posted: 18 April 2018 doi:10.20944/preprints201804.0235.v1

Peer-reviewed version available at Processes 2018, 6, 52; doi:10.3390/pr6050052

The obtained results showed that the gained thermal power in the month January, February, November, and December is less than the rest eight months of the year due to low DNI and the high cosine effect. However, the four months, which have the lowest value of useful thermal power still has the significant potential to provide a thermal power to the system. The selecting solar irradiance around ($500\ W/m^2$) at design point to calculate the total area of collectors can give a great chance for these four months to contribute efficiently to supply a sufficient thermal power, despite a low value of average direct normal irradiance in the region that selected as a case study. In the same direction, the eight months, which have a higher DNI can be exploited to provide direct thermal power to MED and a surplus thermal power to a thermal storage system. Indeed, the optimal area of collectors and storage system capacity are based on the minimum total annual cost of the entire system that can be obtained through an optimization solution.

The monthly distribution of the optimal thermal power mix for MED plant and the entire system has been determined for the different percentage contribution of RO and MED in the total desalinated water production. The optimal thermal power mix for MED plant includes the direct thermal power of solar field, the indirect thermal power of thermal storage system, the surplus thermal power of cogeneration system, and the direct thermal from the combustion of fossil fuels. The monthly distribution varies over the year due to the availability of DNI and the variability of an incident angle, as shown in Figures 4-6.

Preprints (www.preprints.org) | NOT PEER-REVIEWED | Posted: 18 April 2018 doi:10.20944/preprints201804.0235.v1

Peer-reviewed version available at *Processes* **2018**, *6*, 52; doi:10.3390/pr6050052

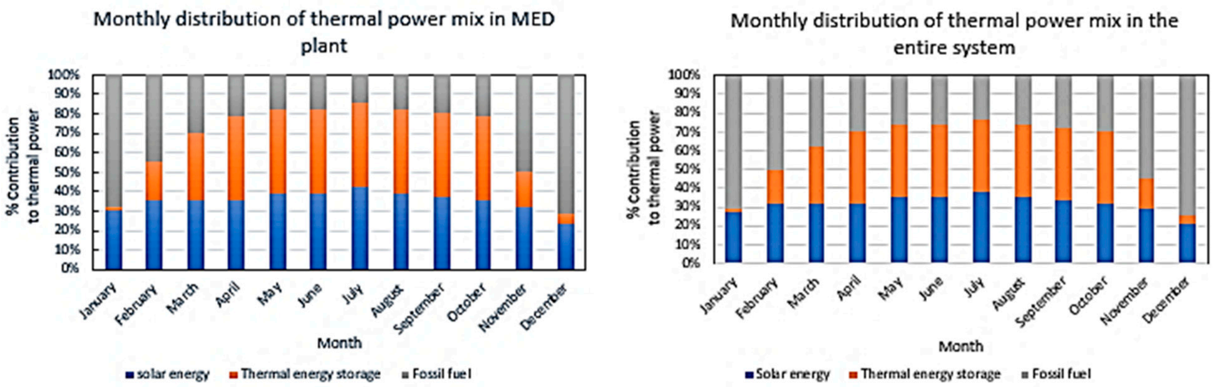

Figure 4: Optimal thermal power mix for MED plant and the entire system with (30% RO 70% MED)

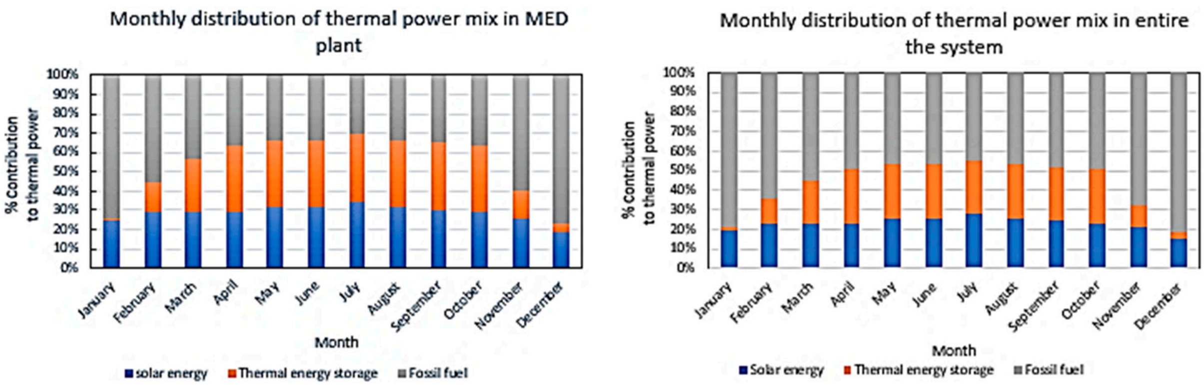

Figure 5: Optimal thermal power mix for MED plant and the entire system with (60% RO 40% MED)

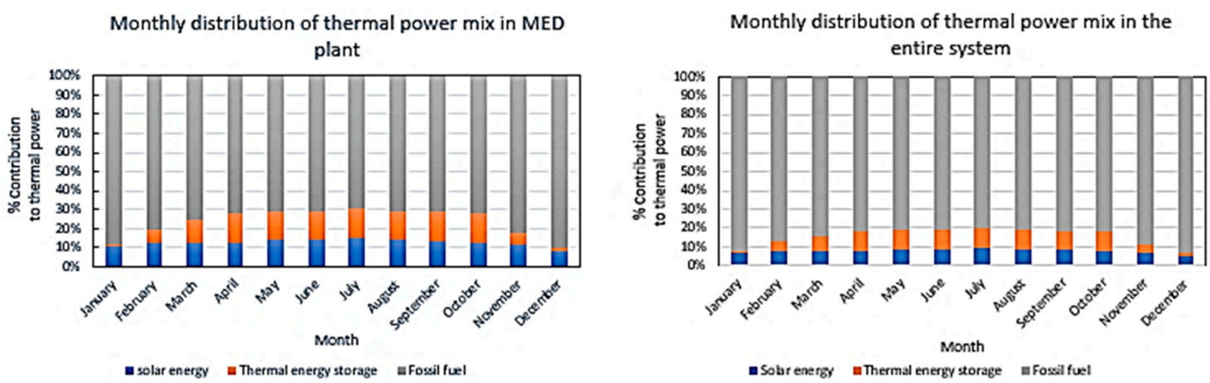

Figure 6: Optimal thermal power mix for MED plant and the entire system with (80% RO 20% MED)

Peer-reviewed version available at Processes 2018, 6, 52; doi:10.3390/pr6050052

The solution of the case study introduces two scenarios to the optimal operation for MED in accordance with the availability of solar energy regardless of the percentage contribution of MED, the first scenario is for the months of January, February, November, and December and shows that it favors the harness of direct solar thermal power during the hours of the diurnal and utilize fossil fuel in the early hours of the day and in the evening. However, stored solar thermal power can be contributed from 1 to 2 hours only because of lacking solar energy in these months, as illustrated in Figure 7, adapted from [43].

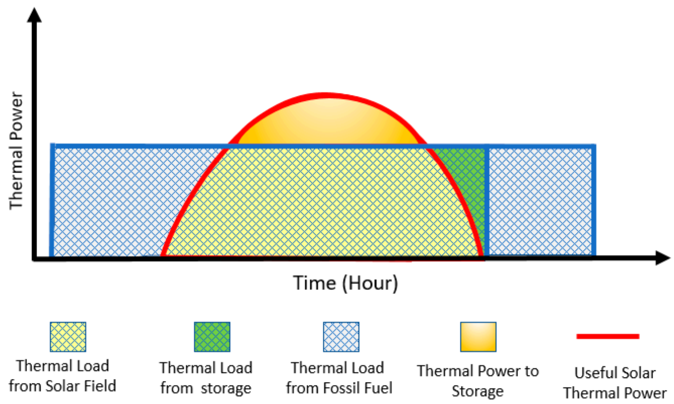

Figure 7: Optimal operation for MED during January, February, November, and December

The second scenario is for the months of April, March, May, June, July, August, December, and October and shows sharply diminishing in using fossil fuel up to 2 hours only. Typically, direct solar thermal power is exploited in the middle of the day while stored solar thermal power is dispatched in the early hours and in the evening, as shown in Figure 8, adapted from [43]. In the future work, the previous two scenarios can be applied to the entire system in the case of integrating solar energy to cogeneration process.

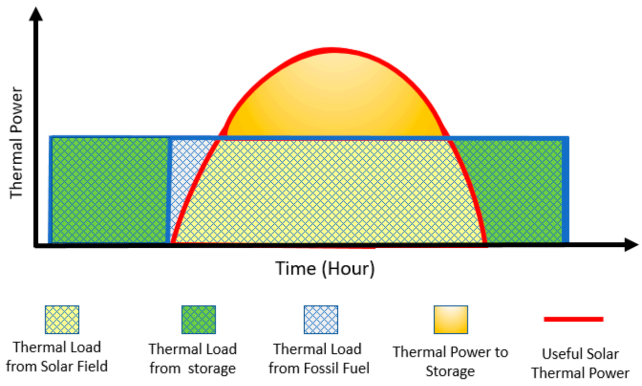

Figure 8: Optimal operation for MED during April, March, May, June, July, August, December, and October

It is observed that the total annual cost of the system as mentioned in the previous section can be reduced by increasing the percentage contribution of RO over MED, but it requires consuming much amount of fossil fuel. More consumption of fossil fuel causes serious environmental impacts due to emitting a massive amount of CO_2. From the case study, the sustaining of fossil fuel resources and diminishing the emissions of greenhouse gas requires enhancing the percentage contribution of MED in the system that based on solar energy as a provider for a high percentage of thermal power. Figure 9 offers an obvious comparison between the economic and environmental aspects of the system through the different percentage contribution of RO and MED in the total desalinated water production. Reconciliation of economic and environmental objective can be achieved using a sustainability weighted return on investment calculation [44, 45].

Peer-reviewed version available at Processes 2018, 6, 52; doi:10.3390/pr6050052

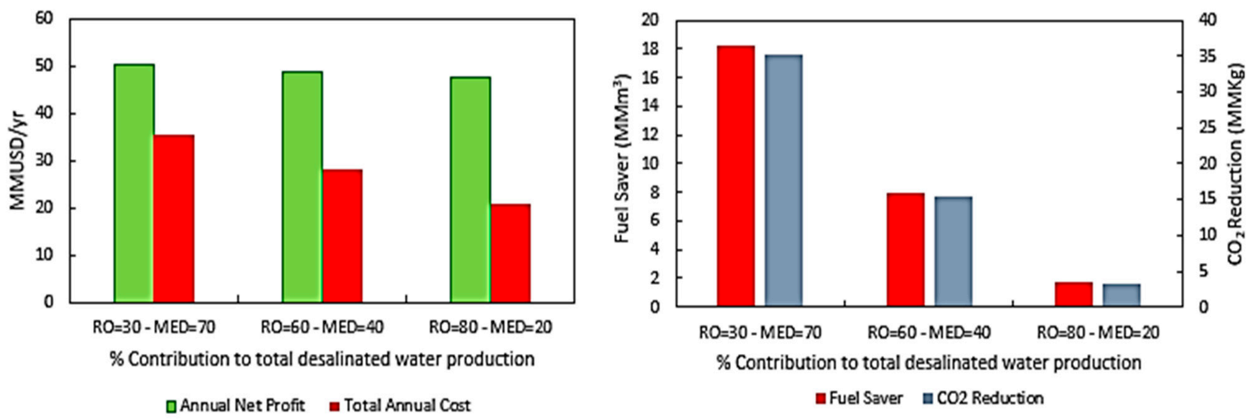

Figure 9: Comparison between the economic and environmental aspects

The case study shows that in Eagle Ford fields, 4.4 billion cubic feet of gas was flared in 2013 that represented around 13% of the gas in the formation [41]. Therefore, this significant amount of flared gas can be exploited as a major source of energy for the system or sharing shale gas in a specific percentage as a minor source of energy, the results of the different percentage contribution of flared gas are shown in Table 5:

Table 5: Technical and economic results for the system

Percentage of Contribution *(%)	Percentage of Contribution **(%)	Total annual cost ($MM\ \$/year$)	$Annual\ Net\ (After - Tax) profit$ ($MM\$/year$)	ROI (%)	Payback period ($year$)
30 RO 70 MED	0.0	35.3	50.4	14.9	5.9
30 RO 70 MED	50	35.1	50.6	14.96	5.6
30 RO 70 MED	100	34.8	50.8	15	5.5
60 RO 40 MED	0.0	28.1	48.8	17.2	4.9
60 RO 40 MED	50	27.8	49	17	4.8
60 RO 40 MED	100	27.5	49.2	17.3	4.8
80 RO 20 MED	0.0	23.5	47.7	19.1	4.4
80 RO 20 MED	50	23.2	47.9	19.2	4.3
80 RO 20 MED	100	22.8	48.1	19.3	4.3

Peer-reviewed version available at *Processes* **2018**, *6*, 52; doi:10.3390/pr6050052

*The percentage contribution of RO and MED plants in the total desalinated water production

** The percentage contribution of flared gas as source of energy

CONCLUSIONS

A water-energy nexus framework has been used to address water management in shale gas production. The following key elements have been integrated: solar energy, fossil fuel, cogeneration process, MED and RO. A hierarchical approach and a multi-period MINLP have been developed and solved to find the optimal mix of solar energy, thermal storage, and fossil fuel and the optimal usage of water treatment technologies. A case study for Eagle Ford Basin in Texas has been solved to show the applicability of the proposed approach. The system has been analyzed according to technical, economic, and environmental aspects. The multi-period method has been applied to discretize the operational period to track the diurnal fluctuations of solar energy. The percentage utilization of water treatment technologies has been iteratively discretized. Once the solution of the mixed integer nonlinear program (MINLP) was applied to each discretization, the optimal mix of solar energy, thermal storage, and fossil fuel, the optimal values of the design and operating variables of the system (e.g., minimum area of a solar collector, maximum capacity of a thermal storage system, etc.) have been determined. The results show that the system the economic and environmental merits of using a water-energy nexus framework and enabling effective water management strategies while incorporating renewable energy.

Peer-reviewed version available at *Processes* **2018**, *6*, 52; doi:10.3390/pr6050052

NOMENCLATURE

a_o, a_1, a_2, a_3	Correlation constants
a, b, and c	Coefficients for the LS-3 collector
AFC^{MED}	Annualized fixed capital cost of the multi-effect desalination
AFC^{RO}	Annualized fixed capital cost of the reverse osmosis
AFC^{SC}	Annualized fixed capital cost of the solar collector
AFC^{cogen}	Annualized fixed capital cost of the cogeneration system
A^{SC}	Effective surface area of the solar collector
A_{SF}	Solar field aperture area
AFC	Total annual fixed cost
AOC	Total annual operating cost
A and B	Parameters that depend on the type of the turbine
bbl	Barrel
c^{Waste}	Value of avoided cost of discharging wastewater
$c_{t,m}^{Fossil}$	Value of fossil fuel
C_{DS}	Disposal cost per volume unit
C_F	Fuel cost per thermal power unit
C_{FW}	Fresh water cost per volume unit
C_{OM}	Operation and maintenance cost per thermal power unit
C_{PST}	Primary and secondary treatment cost per volume unit
C_{SF}	Solar field cost per area unit
C_{SG}	Steam generator system cost per thermal power unit
C_{TES}	Thermal storage system cost per thermal power unit
C_{TR}	Transportation cost per volume unit
$Cp_{,ms}$	Specific heat of the molten salt
Cp_{oil}	Specific heat of oil
do	Outer diameter of the receiver pipe
$D_{t,m}^{Tutbine}$	Design variable of the turbine
DNI	Direct normal irradiance

Preprints (www.preprints.org) | NOT PEER-REVIEWED | Posted: 18 April 2018 doi:10.20944/preprints201804.0235.v1

Peer-reviewed version available at Processes 2018, 6, 52; doi:10.3390/pr6050052

e_{MED}	Electric energy requirements of MED
e_{RO}	Electric energy requirements of RO
E_T	Turbine shaft power output
$E_{t,m}^{Total}$	Electric energy provided by the cogeneration turbine
ft^3	Cubic feet
f	Focal length of the collectors
FCI_B	Fixed capital cost of a boiler
FCI_{PST}	Fixed capital cost of the primary and secondary treatment
FCI_{SF}	Total fixed capital cost of the solar field
FCI_{SG}	Fixed capital cost estimation of the steam generator system
FCI_T	Fixed capital cost of the turbine
FCI_{TES}	Fixed capital cost of the thermal storage system
FCI_{Total}	Total fixed capital cost
F_f	Soiling factor (mirror cleanliness)
FPW	Flowback and produced water
$F_{t,m}^{Fossil}$	Volumetric flow rate of fossil fuel
$F_{t,m}^{MED}$	Volumetric flow rate of desalinated water from MED
$F_{t,m}^{RO}$	Volumetric flow rate of desalinated water from RO
h_{act}^{out}	Actual outlet enthalpy of the turbine
h^{in}	Inlet enthalpy of the steam
h_{is}^{out}	Outlet isentropic enthalpy
HCE	Sum of heat collection element
$K(\Theta)$	Incidence angle modifier
L_{SCA}	Length of a single collector assembly
$L_{spacing}$	Length of spacing between troughs
$\dot{m}$	Inlet turbine steam flowrate
m^{max}	Maximum mass flowrate of the turbine
m_{ms}	Mass flow rate of molten salt
m_{oil}	Mass flowrate of oil

 doi:10.20944/preprints201804.0235.v1

Peer-reviewed version available at Processes 2018, 6, 52; doi:10.3390/pr6050052

MED	Multi-effect distillation plant
$MINLP$	Mixed integer nonlinear program
MM	Million
N_P	Factor to account for the operation pressure of the boiler
N_T	Factor accounting for the superheat temperature of the boiler
N	Service life of the property in years
$NSRDB$	National Solar Radiation Data Base
OC_{OM}	Operation and maintenance cost
O_{EL}	Optical end loss
OC_F	Cost of fuel
$O_{t,m}^{Turbine}$	Operation variable of the turbine
$OPEX_{t,m}^{MED}$	Annualized operational expenditure of MED
$OPEX_{t,m}^{RO}$	Annualized operational expenditure of RO
$OPEX_{t,m}^{SC}$	Annualized operational expenditure of the solar collector
$OPEX_{t,m}^{SC-storage}$	Annualized operational expenditure of the thermal storage system
$OPEX_{t,m}^{cogen}$	Annualized operational expenditure of the cogeneration system
P_g	Gauge pressure of the boiler
PTC	Parabolic trough collector
q_{MED}	Thermal energy requirements of MED
Q_{Boiler}	Thermal power output of the boiler rate
Q_{LFP}:	Thermal power that loss from the headers (pipes)
Q_{LFV}	Thermal power that loss from the expansion tank (vessel)
Q_{TES}	Net thermal power inside the tank
Q_{in}	Inlet thermal power
Q_B	Amount of thermal power that produced by the boiler
Q_{acc}	Accumulated thermal power in the tank from preceding iterations
$Q_{collector\rightarrow ambient}$	Total thermal power that loss from a collector to ambient
$Q_{collector\rightarrow fluid}$	Thermal power that transferred from a collector to a fluid

Preprints (www.preprints.org) | NOT PEER-REVIEWED | Posted: 18 April 2018 doi:10.20944/preprints201804.0235.v1

Peer-reviewed version available at *Processes* **2018**, *6*, 52; doi:10.3390/pr6050052

$Q_{collector \to reciever}$	Thermal power that absorbed by the receiver tube of a collector loop
Q_{out}	Outlet thermal power
$Q_{solar\ field \to final\ demand}$	Useful thermal power that produced by the solar field
$Q_{sun \to collector}$	Solar thermal power that produced by the solar field
Q_{loss}	Thermal power loss
$Q_{t,m}^{Direct,SC}$	Direct thermal power from the solar thermal collector
$Q_{t,m}^{Fossil}$	Direct thermal power from the combustion of fossil fuels
$Q_{t,m}^{In\_Stored-SC}$	Inlet thermal power of the thermal storage system
$Q_{t,m}^{Out\_Stored\_SC}$	Indirect thermal from solar energy through the thermal storage system
$Q_{t,m}^{SC}$	Thermal power captured by the solar collector
$Q_{t,m}^{Stored-Loss}$	Loss thermal power of the thermal storage system
$Q_{t,m}^{Stored-SC}$	Thermal power stored in the thermal storage system
$Q_{t,m}^{Total}$	Total thermal power needs for water treatment
$Q_{t,m}^{Turbine}$	Thermal power from steam leaving the cogeneration turbine
$Q_{t-1,m}^{Stored-SC}$	Thermal power stored from previous iterations
R_{SL}	Row shadow loss
RO	Reverse osmosis plant
ROI	Return on investment
SC	Number of storage capacity hours
T_{CT}	Cold tank temperature
T_{HT}	Hot tank temperature
T_{SH}	Superheat temperature
T_{amb}	Ambient air temperature
T_{in}	Temperature at the inlet of the turbine
T_{ms}	Temperature of the molten salt
T_{rec}	Mean receiver pipe temperature
T_{sat}^{in}	Saturation temperature at the inlet of a turbine
U_{rec}	Overall heat transfer coefficient of the receiver pipe

Peer-reviewed version available at Processes 2018, 6, 52; doi:10.3390/pr6050052

W_c	Width of the collector aperture
W_w	Volumetric flow rate of discharging wastewater
W	Watt

Subscript and superscript symbols

ac	Actual
acc	Accumulated
amb	Ambient
B	Boiler
c	Collector aperture
Cogen	Cogeneration process
CT	Cold tank
DS	Disposal
EL	End loss
f	Factor
F	Fuel
FW	Freshwater
g	Gauge
HT	Hot tank
is	Isentropic
LFP	Loss from pipes
LFV	Loss from vessel
m	Time period (month)
MED	Multi-effect distillation plant
ms	Molten salt
OM	Operation and maintenance
P	Pressure
PST	Primary and secondary treatment
rec	Receiver

Peer-reviewed version available at *Processes* **2018**, *6*, 52; doi:10.3390/pr6050052

RO	Reverse Osmosis plant
sat	Saturation
SC	Solar collector
SCA	Single collector assembly
SF	Solar field
SG	Steam generator
SH	Superheat
SL	Shadow loss
t	Time period (hr)
T	Turbine
TES	Thermal energy storage
TR	Transportation
w	wastewater

Greek symbols

η_{boiler}	Efficiency of the boiler
η_{is}	Isentropic efficiency of the steam turbine
a_Y	Annual operation time
$\Omega_{t,m}^{Turbine}$	Vector set of the turbine
$v_{t,m}^{MED}$	Value of produced water from MED
$v_{t,m}^{RO}$	Value of produced water from RO
$\forall m$	For every month (operational period)
$\forall t$	For every hour (sub- period)
Δh_{is}	Isentropic enthalpy change
η_{opt}	Peak optical efficiency of a collector
θ	Solar incidence angle
θz	Solar zenith angle
γ	Intercept factor
δ	Declination

ΔT	Difference between inlet and outlet of the oil
ρ	Reflectivity
τ	Glass transmissivity
ω	Hour angle
α	Absorptivity of the receiver pipe

REFERENCES

1. Zhang, C. and M. M. El-Halwagi, "Estimate the Capital Cost of Shale-Gas Monetization Projects", Chem. Eng. Prog., 113(12), 28-32 (2017)
2. Al-Douri, A., D. Sengupta, and M. M. El-Halwagi, "Shale Gas Monetization - A Review of Downstream Processing to Chemicals and Fuels", Journal of Natural Gas Science & Engineering, 45, 436-455 (2017)
3. Ortiz-Espinoza, A. P., A. Jiménez-Gutiérreza, M. Nourledin, and M. M. El-Halwagi, "Design, Simulation and Techno-Economic Analysis of Two Processes for The Conversion of Shale Gas to Ethylene", Comp. Chem. Eng., 107, 237-246 (2017)
4. Pérez-Uresti, S.I., Adrián-Mendiola, J.M., El-Halwagi, M.M. and Jiménez-Gutiérrez, "A Techno-Economic Assessment of Benzene Production from Shale Gas", *Processes*, 5(3), 33-42 (2017)
5. Jasper, S. and M. M. El-Halwagi, "A Techno-Economic Comparison of Two Methanol-to-Propylene Processes", *Processes*, 3, 684-698 (2015)
6. Julián-Durán, L., A. P. Ortiz-Espinoza, M. M. El-Halwagi and A. Jiménez-Gutiérrez, "Techno-economic assessment and environmental impact of shale gas alternatives to methanol", ACS Sustainable Chemistry and Engineering 2 (10), pp 2338–2344 (2014)
7. Salkuyeh, Y. K., and T. A. Adams II. "A novel polygeneration process to co-produce ethylene and electricity from shale gas with zero CO2 emissions via methane oxidative coupling." Energy Conversion and Management 92 (2015): 406-420.
8. Ehlinger, V. M., K. J. Gabriel, M. M. B. Noureldin, and M. M. El-Halwagi, "Process Design and Integration of Shale Gas to Methanol", ACS Sustainable Chem. Eng., 2(1), 30-37 (2014)
9. Salkuyeh, Y. K. and Thomas A. Adams II. "Shale gas for the petrochemical industry: Incorporation of novel technologies." In *Computer Aided Chemical Engineering*, vol. 34, pp. 603-608. Elsevier, 2014.
10. Hasaneen, R. and M. M. El-Halwagi, "Integrated Process and Microeconomic Analyses to Enable Effective Environmental Policy for Shale Gas in the United States", Clean Technologies and Environmental Policy, 19(6), 1775-1789 (2017)
11. Arredondo-Ramírez, K, J. M. Ponce-Ortega, and , M. M. El-Halwagi, "Optimal Planning and Infrastructure Development of Shale Gas", Energy Conversion and Management, 119, 91-100 (2016)

Preprints (www.preprints.org) | NOT PEER-REVIEWED | Posted: 18 April 2018 doi:10.20944/preprints201804.0235.v1

Peer-reviewed version available at *Processes* **2018**, *6*, 52; doi:10.3390/pr6050052

12. Gao, J. and F. You (2015). "Optimal design and operations of supply chain networks for water management in shale gas production: MILFP model and algorithms for the water-energy nexus." AIChE Journal 61(4): 1184-1208.
13. Carrero-Parreño, A., V. C. Onishi, R. Salcedo-Díaz, R. Ruiz-Femenia, E. S. Fraga, J. A. Caballero and J. A. Reyes-Labarta (2017). "Optimal Pretreatment System of Flowback Water from Shale Gas Production." Industrial & Engineering Chemistry Research 56(15): 4386-4398.
14. Yang, L., I. E. Grossmann and J. Manno (2014). "Optimization models for shale gas water management." AIChE Journal 60(10): 3490-3501.
15. Nicot, J.-P. and B. R. Scanlon (2012). "Water Use for Shale-Gas Production in Texas, U.S." Environmental Science & Technology 46(6): 3580-3586.
16. Elsayed, N. A., M. A. Barrufet, F. T. Eljack, and M. M. El-Halwagi, "Optimal Design of Thermal Membrane Distillation Systems for the Treatment of Shale Gas Flowback Water", International Journal of Membrane Science and Technology, 2, 1-9 (2015)
17. Boschee, P. (2014). "Produced and Flowback Water Recycling and Reuse: Economics, Limitations, and Technology." SPE-0214-0016-OGF 3(01).
18. Lira-Barragán, L., J. M. Ponce-Ortega, G. Guillén-Gosálbez, and M. M. El-Halwagi, "Optimal Water Management under Uncertainty for Shale Gas Production", Ind. Eng. Chem. Res., 55 (5), 1322–1335 (2016)
19. Chen, H. and K. E. Carter (2016). "Water usage for natural gas production through hydraulic fracturing in the United States from 2008 to 2014." Journal of environmental management 170: 152-159.
20. Shaffer, D. L., L. H. Arias Chavez, M. Ben-Sasson, S. Romero-Vargas Castrillón, N. Y. Yip and M. Elimelech (2013). "Desalination and reuse of high-salinity shale gas produced water: drivers, technologies, and future directions." Environmental science & technology 47(17): 9569-9583.
21. Tovar-Facio, J., F. Eljack, J. M. Ponce-Ortega and M. M. El-Halwagi (2016). "Optimal Design of Multiplant Cogeneration Systems with Uncertain Flaring and Venting." ACS Sustainable Chemistry & Engineering 5(1): 675-688.
22. El-Halwagi, M. M., "Sustainable Design through Process Integration: Fundamentals and Applications to Industrial Pollution Prevention, Resource Conservation, and Profitability Enhancement", Second Edition, IChemE/Elsevier (2017)
23. Khor, C. S., D. C. Y. Foo, M. M. El-Halwagi, R. R.Tan, and N. Shah, "A Superstructure Optimization Approach for Membrane Separation-Based Water Regeneration Network Synthesis with Detailed Nonlinear Mechanistic Reverse Osmosis Model", Ind. Eng. Chem. Res., 50(23), 13444-13456 (2011)
24. Alnouri, S., P. Linke, and M. M. El-Halwagi, "Synthesis of Industrial Park Water Reuse Networks Considering Treatment Systems and Merged Connectivity Options", Comp. Chem. Eng., 91, 289-306 (2016)
25. El-Halwagi, A. M., V. Manousiouthakis and M. M. El-Halwagi, 1996, "Analysis and Simulation of Hollwo Fiber Reverse Osmosis Modules", Sep. Sci. Tech., 31(18), 2505-2529
26. El-Halwagi, M. M., 1992, "Synthesis of Optimal Reverse-Osmosis Networks for Waste Reduction", AIChE J., 38(8), 1185-1198.

Peer-reviewed version available at *Processes* **2018**, *6*, 52; doi:10.3390/pr6050052

27. Goswami, D. Y. and F. Kreith (2007). Energy conversion, CRC press.
28. Mittelman, G. and M. Epstein (2010). "A novel power block for CSP systems." Solar Energy 84(10): 1761-1771.
29. Eck, M., T. Hirsch, J. F. Feldhoff, D. Kretschmann, J. Dersch, A. G. Morales, L. Gonzalez-Martinez, C. Bachelier, W. Platzer and K.-J. Riffelmann (2014). "Guidelines for CSP yield analysis–optical losses of line focusing systems; definitions, sensitivity analysis and modeling approaches." Energy Procedia 49: 1318-1327.
30. Channiwala, S. and A. Ekbote (2015). A generalized model to estimate field size for solar-only parabolic trough plant, 3rd Southern African Solar Energy Conference, South Africa, 11-13 May, 2015.
31. Lovegrove, K. and W. Stein (2012). Concentrating solar power technology: principles, developments and applications, Elsevier.
32. Quaschning, V., R. Kistner and W. Ortmanns (2002). "Influence of direct normal irradiance variation on the optimal parabolic trough field size: A problem solved with technical and economical simulations." TRANSACTIONS-AMERICAN SOCIETY OF MECHANICAL ENGINEERS JOURNAL OF SOLAR ENERGY ENGINEERING 124(2): 160-164.
33. Herrmann, U. and D. W. Kearney (2002). "Survey of thermal energy storage for parabolic trough power plants." TRANSACTIONS-AMERICAN SOCIETY OF MECHANICAL ENGINEERS JOURNAL OF SOLAR ENERGY ENGINEERING 124(2): 145-152.
34. Al-Azri, N., M. Al-Thubaiti, and M. M. El-Halwagi, "An Algorithmic Approach to the Optimization of Process Cogeneration", J. Clean Tech. and Env. Policy, 11(3), 329-338 (2009)
35. Mavromatis, S. and A. Kokossis (1998). "Conceptual optimisation of utility networks for operational variations—I. Targets and level optimisation." Chemical Engineering Science 53(8): 1585-1608.
36. Bamufleh, H. S., J. M. Ponce-Ortega and M. M. El-Halwagi (2013). "Multi-objective optimization of process cogeneration systems with economic, environmental, and social tradeoffs." Clean Technologies and Environmental Policy 15(1): 185-197.
37. Kondash, A. J., E. Albright and A. Vengosh (2017). "Quantity of flowback and produced waters from unconventional oil and gas exploration." Science of the Total Environment 574: 314-321.
38. Atilhan, S., P. Linke, A. Abdel-Wahab, M.M. El-Halwagi, "A Systems Integration Approach to the Design of Regional Water Desalination and Supply Networks", International Journal of Process Systems Engineering (IJPSE), 1(2), 125-135 (2011)
39. Laboratory, N. R. E. (2003). Assessment of parabolic trough and power tower solar technology cost and performance forecasts, DIANE Publishing.
40. Price, H. (2003). A parabolic trough solar power plant simulation model. ASME International Solar Energy Conference, Kohala Coast, HI, March.
41. Horwitt, D. and L. Sumi (2014). "Up in Flames: US Shale Oil boom comes at Expense of Wasted Natural Gas, Increased CO2." Earthworks, Washington, DC, USA.
42. Division, S. R. E. E. (2015). "Advanced treatment of shale gas fracturing water to produce re-use or discharge quality water." Retrieved November,2017, from http://www.rpsea.org/media/files/project/6e557d38/11122-57-FR-

Advanced_Treatment_Shale_Gas_Fracturing_Produce_NPDES_Quality_Water-11-30-15_P.pdf.[41]

43. Giuliano S, Buck R, Eguiguren S, "Analysis of solar-thermal power plants with thermal energy storage and solar-hybrid operation strategy", Journal of Solar Energy Engineering 3, 133 (2011)

44. El-Halwagi, M. M., "A Return on Investment Metric for Incorporating Sustainability in Process Integration and Improvement Projects", Clean Technologies and Environmental Policy, 19:611-617 (2017)
45. Guillen-Cuevas, K. A. P. Ortiz-Espinoza, E. Ozinan, A. Jiménez-Gutiérrez, N. K. Kazantzis, M. M. El-Halwagi, "Incorporation of Safety and Sustainability in Conceptual Design via A Return on Investment Metric ", ACS Sustainable Chemistry and Engineering 6, 1411-1416 (2018)

Preprints (www.preprints.org) | NOT PEER-REVIEWED | Posted: 18 April 2018 doi:10.20944/preprints201804.0235.v1

Peer-reviewed version available at Processes 2018, 6, 52; doi:10.3390/pr6050052

APPENDIX I: SOLAR DATA FOR THE CASE STUDY

The solar data for Eagle Ford Shale Play as extracted from National Solar Radiation Data Base (NSRDB) are shown by Tables I.1-I.4 to represent:

- Average hourly dry bulb temperature ($°C$)
- Average hourly wet bulb temperature ($°C$)
- Average hourly direct solar irradiance (W/m^2)
- Average hourly solar incidence angle (degree)

The solar beam radiation is 500 (W/m^2) at a design point.

Table I.1: Average hourly dry bulb temperature ($°C$)

Month / Hour	January	February	March	April	May	June	July	August	September	October	November	December
0.5	7.1	8.1	13.4	17.3	20.9	23.6	13.4	25.1	24.1	18.9	13.1	8.2
1.5	6.6	7.71	13.0	16.9	20.4	23.3	13.0	24.5	23.6	18.2	12.6	7.7
2.5	6.1	7.24	12.6	16.4	19.9	23.1	12.6	24.0	23.2	17.4	12.3	7.36
3.5	6.0	6.98	12.3	16.2	19.6	23.0	12.3	23.6	22.9	17.1	11.6	7.11
4.5	5.9	6.74	12.0	16.0	19.3	22.8	12.0	23.2	22.6	16.8	11.4	7.13
5.5	5.9	6.49	11.7	15.8	19.0	22.8	11.7	22.8	22.4	16.5	11.3	6.96
6.5	5.5	7.37	12.6	16.8	20.1	23.3	12.6	24.2	22.4	17.9	10.9	7.03
7.5	5.4	8.28	13.5	17.8	21.2	24.6	13.5	25.6	23.7	19.3	11.8	7.21
8.5	7.7	9.20	14.5	18.8	22.3	26.0	14.5	27.0	25.6	20.6	14.0	9.10
9.5	10	11.1	16.2	20.1	23.4	27.3	16.2	28.5	27.0	22.1	16.3	11.0
10.5	12	13.0	17.9	21.4	24.5	28.4	17.9	30.1	28.2	23.6	18.0	12.8
11.5	13	14.9	19.6	22.7	25.6	29.4	19.6	31.6	29.4	25.2	19.3	14.1
12.5	14	15.7	20.5	23.5	26.2	30.4	20.5	32.4	30.3	25.8	20.3	15.1

Preprints (www.preprints.org) | NOT PEER-REVIEWED | Posted: 18 April 2018 doi:10.20944/preprints201804.0235.v1

Peer-reviewed version available at Processes 2018, 6, 52; doi:10.3390/pr6050052

13.5	15	16.6	21.4	24.4	26.8	31.3	21.4	33.3	30.7	26.5	21.1	16.0
14.5	15	17.5	22.3	25.2	27.5	31.4	22.3	34.1	31.0	27.2	21.3	16.4
15.5	16	17.0	21.7	24.8	27.4	31.7	21.7	33.5	31.2	26.5	21.2	16.5
16.5	15	16.5	21.2	24.4	27.4	31.2	21.2	32.9	31.0	25.8	20.5	16.0
17.5	13	16.1	20.7	23.9	27.3	30.4	20.7	32.3	30.2	25.1	19.0	14.4
18.5	12	14.6	19.1	22.5	26.1	29.0	19.1	30.9	28.8	24.0	17.3	12.7
19.5	10.9	13.21	17.5	21.2	24.95	27.64	17.5	29.53	27.76	22.88	15.84	11.2
20.5	9.73	11.77	16.0	19.8	23.7	26.47	16.0	28.10	26.68	21.75	14.63	10.3
21.5	8.63	10.79	15.3	19.2	23.0	25.44	15.3	27.30	25.93	21.00	13.95	9.77
22.5	7.91	9.825	14.5	18.5	22.3	24.75	14.5	26.46	25.36	20.25	13.45	9.55
	7.56	8.846	13.8	17.7	21.5	24.0	13.8	25.6	24.7	19.6	13.30	9.31

Table I.2: Average hourly wet bulb temperature (°C)

Month / Hour	January	February	March	April	May	June	July	August	September	October	November	December
0.5	5.7	6.3	9.85	15.3	18.5	21.6	22.9	22.0	21.5	16.3	11.4	6.41
1.5	5.4	6.0	9.69	15.1	18.3	21.5	22.8	22.0	21.3	15.9	11.1	6.03
2.5	4.9	5.7	9.52	14.9	18.0	21.4	22.7	21.9	21.2	15.4	10.8	5.75
3.5	4.9	5.5	9.43	14.7	17.8	21.4	22.7	21.8	21.0	15.1	10.2	5.55
4.5	4.8	5.3	9.35	14.6	17.6	21.4	22.6	21.6	20.9	14.9	10.1	5.56
5.5	4.8	5.0	9.21	14.5	17.4	21.4	22.6	21.4	20.8	14.6	10.0	5.40
6.5	4.5	5.7	9.64	15.1	18.1	21.7	22.9	22.0	20.8	15.6	9.78	5.44
7.5	4.3	6.3	10.0	15.7	18.8	22.2	23.3	22.6	21.4	16.4	10.3	5.60
8.5	6.1	7.0	10.4	16.3	19.4	22.6	23.4	23.1	22.0	17.2	11.6	6.99
9.5	7.5	8.0	11.3	17.0	19.8	22.7	23.6	23.4	22.2	17.8	12.7	8.08
10.5	8.4	8.9	12.0	17.6	20.1	22.8	23.6	23.4	22.2	18.3	13.3	8.90
11.5	9.1	9.6	12.5	18.1	20.4	23.0	23.5	23.3	22.1	18.7	13.8	9.42
12.5	9.5	10	12.7	18.4	20.7	23.0	23.5	23.3	22.3	18.8	14.0	9.82

Preprints (www.preprints.org) | NOT PEER-REVIEWED | Posted: 18 April 2018 doi:10.20944/preprints201804.0235.v1

Peer-reviewed version available at Processes 2018, 6, 52; doi:10.3390/pr6050052

13.5	10	10	12.9	18.6	21.0	23.2	23.5	23.2	22.2	18.9	14.2	10.1
14.5	10	10	13.0	18.8	21.2	22.9	23.5	23.0	22.1	19.0	14.1	10.3
15.5	10	10	12.8	18.5	21.1	22.9	23.4	22.8	22.0	18.7	14.1	10.2
16.5	9.8	10	12.5	18.3	20.9	22.8	23.3	22.6	22.0	18.5	13.8	10.0
17.5	9.2	9.8	12.2	18.1	20.7	22.7	23.3	22.3	22.0	18.2	13.3	9.39
18.5	8.6	9.4	11.9	17.6	20.5	22.4	23.4	22.4	21.8	18.0	12.7	8.72
19.5	8.0	8.9	11.4	17.1	20.2	22.3	23.4	22.4	21.8	17.7	12.2	8.13
20.5	7.4	8.3	10.8	16.5	19.8	22.1	23.2	22.1	21.6	17.3	11.7	7.78
21.5	6.9	7.9	10.6	16.3	19.5	22.0	23.2	22.2	21.6	17.1	11.4	7.50
22.5	6.4	7.4	10.3	16.0	19.2	21.9	23.1	22.1	21.6	16.9	11.3	7.37
23.5	6.1	6.8	9.91	15.5	18.7	21.7	22.9	21.9	21.6	16.7	11.4	7.30

Table I.3: Average hourly direct solar irradiance (W/m^2)

Month / Hour	January	February	March	April	May	June	July	August	September	October	November	December
0.5	0	0	0	0	0	0	0	0	0	0	0	0
1.5	0	0	0	0	0	0	0	0	0	0	0	0
2.5	0	0	0	0	0	0	0	0	0	0	0	0
3.5	0	0	0	0	0	0	0	0	0	0	0	0
4.5	0	0	0	0	0	0	0	0	0	0	0	0
5.5	0	0	0	0	5.1	3.8	1	0.0	0	0	0	0
6.5	0	0	9.6	26	109	86	65	57	34	26	1.8	0
7.5	48	95	140	145	216	164	236	229	184	221	171	49
8.5	240	244	287	228	258	319	350	347	315	337	328	199
9.5	339	346	365	281	318	377	467	463	450	460	388	272
10.5	396	413	413	352	362	470	550	524	516	497	462	359
11.5	415	487	478	394	383	496	630	573	557	553	545	389
12.5	473	468	498	439	462	526	621	599	569	566	544	459

Preprints (www.preprints.org) | NOT PEER-REVIEWED | Posted: 18 April 2018 doi:10.20944/preprints201804.0235.v1

Peer-reviewed version available at *Processes* **2018**, *6*, 52; doi:10.3390/pr6050052

13.5	457	474	481	461	460	545	603	600	521	542	504	489
14.5	415	440	417	467	445	520	576	540	540	544	481	499
15.5	397	433	380	473	503	489	529	539	493	498	437	440
16.5	283	365	323	414	434	475	536	417	422	401	361	323
17.5	128	246	234	338	356	389	427	323	311	181	93	80
18.5	0.4	32	54	119	166	217	234	140	53	3.6	0	0
19.5	0	0	0	0.1	7.2	21	24	4.3	0	0	0	0
20.5	0	0	0	0	0	0	0	0	0	0	0	0
21.5	0	0	0	0	0	0	0	0	0	0	0	0
22.5	0	0	0	0	0	0	0	0	0	0	0	0
23.5	0	0	0	0	0	0	0	0	0	0	0	0

Table I.4: Average hourly solar incidence angle (degree)

Month / Hour	January	February	March	April	May	June	July	August	September	October	November	December
0.5	0	0	0	0	0	0	0	0	0	0	0	0
1.5	0	0	0	0	0	0	0	0	0	0	0	0
2.5	0	0	0	0	0	0	0	0	0	0	0	0
3.5	0	0	0	0	0	0	0	0	0	0	0	0
4.5	0	0	0	0	0	0	0	0	0	0	0	0
5.5	0	0	0	0	0	0	0	0	0	0	0	0
6.5	0	0	0	6.04	16.1	20.2	19.2	11.1	0	0	0	0
7.5	0	4.33	7.10	2.51	9.26	13.4	12.3	5.49	4.95	16.1	23.4	0
8.5	30.6	23.6	14.3	4.99	2.85	6.99	5.77	2.49	11.8	23.4	31.8	34.4
9.5	37.8	30.5	20.7	10.9	2.76	1.52	1.14	7.13	18.0	29.8	38.5	41.4
10.5	43.8	36.3	26.1	15.6	7.01	2.69	4.28	11.8	22.9	35.0	44.0	47.1
11.5	48.2	40.6	30.0	18.7	9.73	5.40	7.20	14.9	26.3	38.4	47.6	51.1
12.5	50.2	42.7	31.8	20.0	10.7	6.44	8.40	16.2	27.5	39.3	48.5	52.6

Preprints (www.preprints.org) | NOT PEER-REVIEWED | Posted: 18 April 2018 doi:10.20944/preprints201804.0235.v1

Peer-reviewed version available at *Processes* **2018**, *6*, 52; doi:10.3390/pr6050052

13.5	49.5	42.1	31.0	19.0	9.79	5.70	7.78	15.3	26.2	37.5	46.5	51.1
14.5	46.1	39.0	27.8	16.0	7.06	3.20	5.40	12.7	22.8	33.4	42.2	47.2
15.5	40.7	34.0	22.9	11.5	2.79	0.83	1.58	8.49	17.8	27.8	36.2	41.4
16.5	34.0	27.7	16.9	5.74	2.83	6.15	3.82	3.07	11.7	21.1	29.2	34.4
17.5	21.1	20.4	9.96	2.65	9.23	12.4	10.1	3.61	4.78	11.5	0	0
18.5	0	0	0.17	8.06	16.1	19.2	16.9	10.5	0.99	0	0	0
19.5	0	0	0	0	0	0	0	0	0	0	0	0
20.5	0	0	0	0	0	0	0	0	0	0	0	0
21.5	0	0	0	0	0	0	0	0	0	0	0	0
22.5	0	0	0	0	0	0	0	0	0	0	0	0
23.5	0	0	0	0	0	0	0	0	0	0	0	0